

Comparing $H\beta$ Line Profiles in the 4D Eigenvector 1 Context

J. W. Sulentic

Instituto de Astrofísica de Andalucía, CSIC, Apdo. 3004, 18080 Granada, Spain

P. Marziani

INAF, Osservatorio Astronomico di Padova, Vicolo dell' Osservatorio 5, 35122 Padova, Italy

S. Zamfir

Department of Physics and Astronomy, University of Alabama, Tuscaloosa, AL 35487, USA

Abstract

We describe a 4D Eigenvector 1 (4DE1) space that serves as a surrogate H-R diagram for quasars. It provides a context for describing and unifying differences between all broad line AGN. Quasar spectra can be averaged in a non-random way using 4DE1 just as stellar spectra can be averaged non-randomly within the OBAFGKM classification sequence. We find that quasars with FWHM $H\beta$ less than (Population A) and greater than (Population B) 4000 km s^{-1} show many significant differences that may point to an actual dichotomy. Broad line profile measures and fits reinforce the idea of a dichotomy because they are fundamentally different: Pop.A - Lorentzian-like and Pop.B - double Gaussian. The differences have implications both for BH mass estimation and for inferences about source structure and kinematics.

Key words:

galaxies:active, galaxies:quasars:emission lines, galaxies:quasars:general

1. Introduction

Studies of quasar spectra have fallen out of fashion over the past ten years. This impression is supported by the small number of citations involving optical/UV spectroscopic work found from a random NED search of citations for

even the brightest (e.g., PG) sources. One can identify at least two reasons for this paucity of studies: 1) a widespread belief that all broad-line spectra are essentially the same and/or 2) the impression that a deeper understanding of broad-line phenomenology and physics is unobtainable. The one exception, reflecting reason 1) involves computation of mean/median composite spectra from large samples (e.g. 2dF, SDSS). Of course if reason 1) is not correct then these results will reinforce reason 2). Just as the indiscriminate averaging of OBAFGKM stellar spectra would yield bizarre conclusions. The purpose of this review is to convince the reader that reason 1) is incorrect and that understanding quasar spectral diversity can stimulate new ideas that will remove the sense of hopelessness reflected in reason (2).

The question is how best to represent quasar phenomenological diversity and unite it into a coherent picture. The history of stellar studies immediately comes to mind although quasars are almost certainly more complicated sources. At the very least source orientation to our line-of sight likely adds a serious complication. We have been working on a spectroscopic unification for quasars that, in fact, embraces all broad line emitting AGN. Gradually the hope emerged of finding a diagnostic space capable of serving as a surrogate H-R diagram for quasars. A 2D H-R diagram works quite well because, among other things, stellar orientation plays no major role in spectroscopic studies. The full power of the stellar H-R diagram requires exploitation of more parameter dimensions. Certainly an equivalent spectroscopic diagnostic space for quasars will require more than two dimensions if only to remove the orientation-physics degeneracy. In 2000 we proposed a 4D Eigenvector 1 parameters space (hereafter 4DE1; [Sulentic et al. 2000a](#)). 4DE1 remains the most promising way to emphasize the spectroscopic diversity while also contextualizing the diverse types of broad-line emitting sources.

4DE1 space emphasizes observables with the largest intrinsic dispersions including the most statistically significant line profile differences. 4DE1 has roots in the Principal Component Analysis (PCA) of the Bright (PG) Quasar Sample ([Boroson & Green 1992](#); BG92) as well as in correlations that emerged from ROSAT ([Wang et al. 1996](#)). 4DE1 in its simplest form involves two BG92 measures: 1) full width half maximum of broad $H\beta$ (FWHM $H\beta$) and 2) equivalent width ratio of optical FeII and broad $H\beta$: $R_{FeII} = W(\text{FeII } \lambda 4750 \text{ blend})/W(H\beta)$. We added measures of 3) the soft X-ray photon index (Γ_{soft}) and 4) CIV λ 1549 broad-line profile displacement at half maximum ($c(1/2)$). Other points of departure from BG92 involve comparison of radio-quiet (RQ) sources with a large radio-loud (RL) sample. We also sub-

ordinate $[\text{OIII}]\lambda\lambda 4959,5007$ measures (although see: [Zamanov et al. 2002](#); [Marziani et al. 2003a, 2009](#)). 4DE1 tells us that all quasars are not similar whether we observe them at optical, UV or X-ray wavelengths.

2. The Optical-UV Dimensions of 4DE1 Space

Thus defined 4DE1 includes key measures of both representative high (HIL: $\text{CIV}\lambda 1549$, 65eV) and low (LIL: $\text{H}\beta$, 13.6eV) ionization lines. This is important because LIL and HIL behave very differently. While forming the core of 4DE1 the four adopted key parameters only begin to exploit the fundamental trends and source differences that exist. This review emphasizes results involving 4DE1 parameters describing broad emission line profiles. Figure 1 shows the latest representation of the optical plane of 4DE1 involving FWHM $\text{H}\beta$ and R_{FeII} measures for the 321 brightest ($g < 17.0$) low redshift ($z < 0.7$) quasars (grey dots) in the Sloan Digitized Sky Survey (SDSS; DR5) ([Zamfir et al. 2008](#)). Results are very little different if one adopts an i-band magnitude cutoff. An i-band selection adds many nearby lower luminosity sources with strong host galaxy contamination. SDSS does not recognize sources with $\text{FWHM H}\beta < 1000 \text{ km s}^{-1}$ as quasars motivating us to add to our sample $n=41$ narrow-line Seyfert 1 (NLSy1) sources brighter than $g=17.5$ ($z < 0.7$) identified by [Zhou et al. \(2006\)](#) (black squares). Source occupation is very similar to what was found with our own low redshift atlas sample of 215 sources ([Marziani et al. 2003b](#)). Figure 2 shows an optical-UV plane of 4DE1 involving FWHM $\text{H}\beta$ and $\text{CIV}\lambda 1549$ profile displacement ($c(1/2)$). In this case the CIV measures exhaust the HST archive of available data with $N=130$ low z sources (see [Bachev et al. 2004](#); [Sulentic et al. 2007](#) for details).

Figures 1 and 2 clearly show trends but what do they mean? Does Figure 1 show a continuous or “main” sequence? Or is there evidence for an actual source dichotomy? Even if a dichotomy is not obvious it might be useful to propose one as a means to highlight source difference. A more striking difference is seen when RL (grey circle-dots) and RQ (grey dots) source occupation in 4DE1 is compared in Figure 1. This occupation difference motivates the idea of a dichotomy because almost all RL sources show $\text{FWHM H}\beta > 4000 \text{ km s}^{-1}$ while 50-60% of RQ sources shows smaller values. The alternative interpretation would see RL quasars as a fundamentally different class of quasar that partially overlaps with RQ domain occupation in 4DE1. It really doesn’t matter which interpretation is correct, the RL-RQ difference is an important clue about Broad Line Region (BLR) physics. Other measures

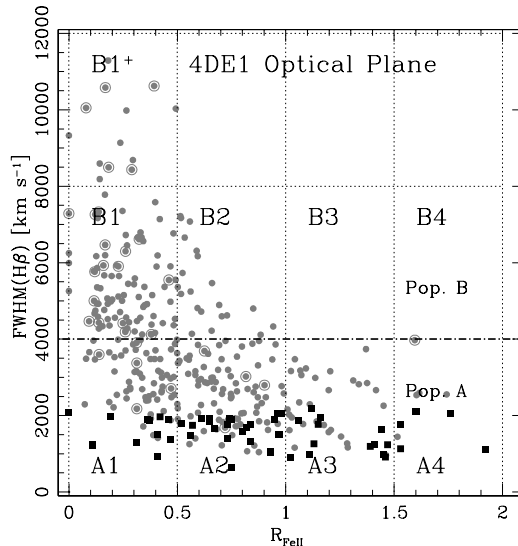


Figure 1: The optical plane of the 4DE1 space. Two populations A and B are separated at $\text{FWHM H}\beta = 4000 \text{ km s}^{-1}$. Bins of $\Delta(\text{FWHM H}\beta) = 4000 \text{ km s}^{-1}$ and $\Delta(R_{\text{FeII}}) = 0.5$ enclose sources that have statistically similar $\text{H}\beta$ width and FeII relative strength. Bins labels follow the convention of [Sulentic et al. \(2002\)](#). Grey symbols indicate RQ sources, circled grey symbols indicate RL quasars and the black symbols indicate the subset of narrow broad line sources extracted from [Zhou et al. \(2006\)](#).

(e.g., $c(1/2)$ and Γ_{soft}) point to a change in source occupation near 4000 km s^{-1} . Figure 2 shows that only sources with $\text{FWHM H}\beta < 4000 \text{ km s}^{-1}$ show a blueshift/asymmetry of the HIL.

These empirical results further motivate the idea of contrasting sources above and below $\text{FWHM H}\beta = 4000 \text{ km s}^{-1}$. The list of source differences, and inferred physical differences, continues to grow (see Table 5 in [Sulentic et al. 2007](#)).

3. Composite Spectra of Populations A and B Quasars

Figures 3 and 4 show median composite spectra for the $\text{H}\beta$ region in the two most highly populated bins indicated in Figure 1 (A2 and B1 respectively). The composites are generated from 128 and 130 sources respectively and illustrate a striking $\text{H}\beta$ line profile difference between Pop. A and B sources. This is an example of averaging quasar spectra in an organized and predefined context. It is the best way to bin the sources without imposing any assumptions about the structure of the BLR. The size of the bins

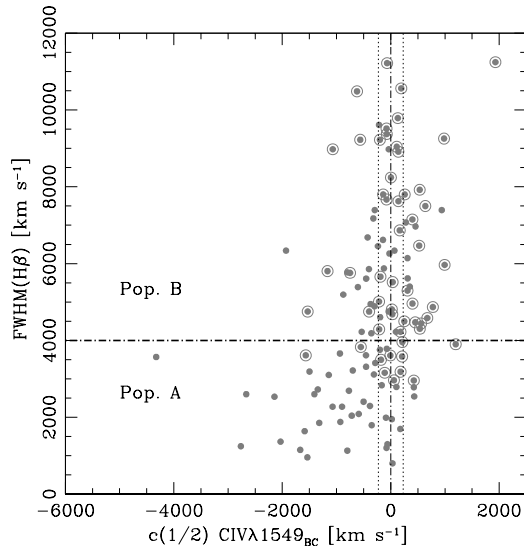


Figure 2: An optical-UV plane of the 4DE1 showing the FWHM $H\beta$ versus the centroid shift of broad component of $CIV\lambda 1549$ (at 1/2 fractional intensity). The symbols are similar to those in Figure 1. The Population A/B 4000 km s^{-1} boundary is also shown.

was driven by the current accuracy of FWHM $H\beta$ and R_{FeII} measures. All sources within a bin therefore have statistically similar FWHM and R_{FeII} values. We think that these median composite spectra, or better said, the differences between them, are the key to a deeper understanding of the quasar BLR and structural differences between sources along the principal sequence in the 4DE1 optical plane. Figure 3 and 4 show that all quasar spectra are not the same. Our 4000 km s^{-1} boundary appears to be much more significant than the $FWHM H\beta = 2000 \text{ km s}^{-1}$ boundary often used to distinguish narrow (NLSy1) and broad (BLSy1) line Seyfert galaxies/quasars. Comparison of sources in 1000 km s^{-1} intervals above and below 2000 km s^{-1} reveals little difference; they are all what we call Pop. A sources and they are all (similarly) different from Pop. B sources. We will consider and contrast Figures 3 and 4 in the next two sections.

It is important to emphasize that the $n \approx 130$ sources going into each median composite show a wide diversity of profile shapes although less for Pop. A than for Pop. B. Naturally we are assuming that 4DE1 measures are first-order discriminators. We also assume that they do not change dramatically with time. Higher-order measures of line shift and shape are known to vary with time. One can study these changes in an individual source via moni-

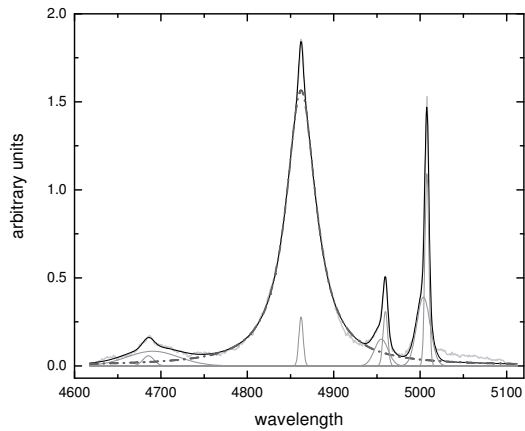


Figure 3: Composite median spectrum of sources in bin A2. The dashed-dotted profile indicates the Lorentzian fit for the broad component of $H\beta$. The $[OIII]\lambda\lambda$ 4959,5007 and $HeII\lambda$ 4686 lines require two Gaussians each.

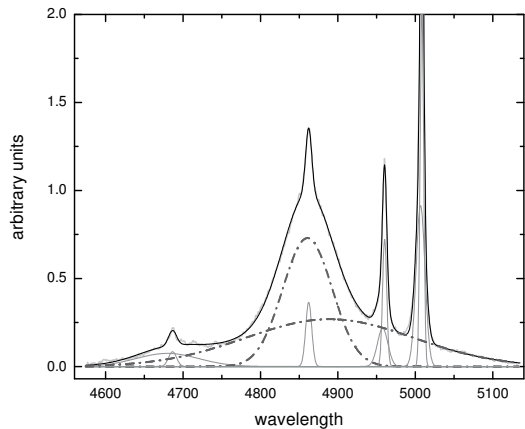


Figure 4: Composite median spectrum of sources in bin B1. The dashed-dotted profiles indicate the two Gaussians (BLR+redshifted VBLR) for $H\beta$. The $[OIII]\lambda\lambda$ 4959,5007 and $HeII\lambda$ 4686 lines are fitted with two Gaussians each.

toring, which costs a lot of observing time. Our alternative approach is to generate median spectra from large enough samples that we will likely catch source profiles in all or most significant states of change. Median composite profiles therefore offer the possibility to isolate the underlying most stable or common profile shape. The shapes that we see in Figures 3 and 4 have appeared in earlier composite spectra that we have generated with smaller and less uniform samples. This gives us confidence that we have isolated

stable characteristics of Pop. A and B $H\beta$ line profiles.

4. Population A Sources

More than half ($\sim 60\%$, [Sulentic et al. 2000a](#); [Zamfir et al. 2008](#)) of a magnitude limited quasar sample satisfies our Pop. A. definition. RL sources are rare in Pop. A with perhaps 2-4% satisfying standard definitions of radio-loudness. Most RL sources show broader Balmer line profiles and we argue that many/most formally Pop. A RL quasars are sources that fall there because they are oriented near face-on to our line of sight. A reasonable correction for orientation, and assumption of a flattened BLR geometry ([Marziani et al. 2001, 2003a](#)), moves them into the Pop. B domain with the bulk of RL quasars.

Figure 3 shows our Pop. A median composite for bin A2. Composites for higher A bins would show even more extreme differences— especially stronger R_{FeII} but would have lower S/N because they include fewer sources as is clear from Figure 1. Once we have generated the composites we face the challenge of modeling them in the simplest way. Over the past 10+ years, and especially for NLSy1, it has been suggested that sources with narrower $H\beta$ profiles can be well fit with a Lorentz function. They can then be described as Lorentz-like profiles. Figure 3 confirms this single-component fit for Pop. A-bin A2 sources. Whatever might be the source-to-source differences there appears to be an underlying stable Lorentz line. This profile shape disappears above $\text{FWHM } H\beta \approx 4000 \text{ km s}^{-1}$.

Figure 2 shows that $\text{CIV } \lambda 1549$ profiles for Pop. A sources are blue shifted. Blueshifts as large as $4\text{-}5000 \text{ km s}^{-1}$ are observed although most Pop. A sources show smaller displacements of less than 500 km s^{-1} . While not individually significant the overall sample displacement certainly is significant especially when compared with the distribution of CIV line shifts in Pop. B. Pop. A-B differences extend to all CIV measures with equivalent width $W(\text{CIV})$ for Pop. A sources about 1/2 the Pop. B value. FWHM CIV shows a smaller range than Pop. B and we find no correlation between $\text{FWHM } H\beta$ and FWHM CIV measures for Pop. A. ([Sulentic et al. 2007](#)). The large differences between $H\beta$ and CIV profiles tell us that the LIL and HIL in Pop. A sources arise in regions with different geometry and kinematics.

The high S/N and resolution of this SDSS-based sample enable us to quantify line asymmetry and shift properties of broad $H\beta$ (see [Zamfir et al.](#)

2009 for definitions of these measures). The distribution of profile asymmetries shows mean/median values consistent with zero asymmetry with a sample standard deviation of ± 0.11 (estimated 2σ measurement uncertainties are ± 0.16). Mean line shift measures at FW1/4 “base” and FW3/4 “peak” are -42 and -41 km s^{-1} respectively. A small fraction ($\sim 5\%$) of Pop. A sources show a weak blue wing that involves sources in bins A3 and A4. These tend to involve sources with the largest CIV blueshifts (Zamfir et al. 2009) suggesting that we may be detecting weak $\text{H}\beta$ emission from the same wind or outflow responsible for the HIL blueshifts.

The bulk of Pop. A $\text{H}\beta$ emission involves profiles that are symmetric, unshifted and Lorentz-like. The soft X-ray excess from these sources has been argued to be a thermal disk signatures in what are thought to be the highest accreting sources. Similarly the CIV blueshift/asymmetry has been ascribed to a disk wind or outflow. Pop. A sources also lie at the high electron density n_e end of the 4DE1 sequence shown in Figure 1 (see also Marziani et al. 2001) with estimated values in the range $\log(n_e[\text{cm}^{-3}]) = 10-11$. All of these results are consistent with the hypothesis that the most important BLR component in Pop. A sources involves a thin/slim accretion disk with n_e and column densities high enough to explain the strong FeII emission in these sources.

Coupled with the $\text{H}\beta$ line profile properties lead us to conclude that FWHM $\text{H}\beta$ is a reliable virial estimator for Pop. A quasars while FWHM CIV is not (Bachev et al. 2004; Sulentic et al. 2007). Estimated black hole masses for Pop. A sources lie in the range $\log(M_{BH}[M_{\odot}])=6.5-8.5$ with inferred Eddington ratios in the range $\log L_{BOL}/L_{EDD} = 0.1-3.0$. The apparent super Eddington radiators can all be corrected to values below 0.9 by assuming that some Pop. A radiators are observed with the line emitting accretion disk oriented near face-on. Reasonable orientation corrections (Marziani et al. 2003a) increase the smallest M_{BH} estimates to values above 7.0 thus reducing extreme L_{BOL}/L_{EDD} values to the sub-Eddington range.

5. Population B Sources

A description of population B sources will be different from the above pop. A description in virtually every measurable parameter. This includes emission line profiles and a comparison of Figures 3 and 4 makes it clear. Pop. B includes the bulk of the RL quasars and about 25% of the RQ sources. The probability of radio-loudness in Pop. B is about 4-5 times higher than for

Pop. A (Marziani et al. 2003a; Zamfir et al. 2008). The meaning of this RQ-RL overlap region in 4DE1 is unclear but there are two obvious possibilities: 1) RL sources represent a distinct quasar class that partially overlaps the RQ domain or 2) about 25% of RQ quasars show geometry and kinematics identical to RL quasars. They might be RL pre- and/or post-cursors or their central geometry may be the same as RL galaxies, but either host galaxy morphology or black hole spin prevents their becoming RL.

Figure 4 shows our median composite for bin B1 marked in Figure 1. It represents a median composite of about 130 quasars. The S/N of the Figure 3 and 4 spectra are similar, about 130. The median source luminosity in the two bins $\log(L_{BOL}[\text{erg s}^{-1}])=45.7$ are also the same (median redshifts 0.30 and 0.28 for bins A2 and B1 respectively). It is immediately obvious that the bin B1 $H\beta$ profile cannot be fit with a Lorentz function. Previous studies with our atlas sample (Marziani et al. 2003b) required a minimum of two Gaussian components to model the $H\beta$ profile after FeII subtraction, unshifted BLR + redshifted Very Broad component VBLR (Sulentic et al. 2002). Figure 4 shows that the double Gaussian fit again matches well the $H\beta$ profile in our SDSS composite spectrum. If we separate Pop. B sources into luminosity bins we find that FWHM $H\beta$ increases with source luminosity from 5200 km s^{-1} ($\log(L_{BOL}[\text{erg s}^{-1}])=43-44$) to 9300 km s^{-1} ($\log(L_{BOL}[\text{erg s}^{-1}])=48-49$) (Marziani et al. 2009). If we correct for the VBLR component $\text{FWHM } H\beta \approx 10^4 \text{ km s}^{-1}$ redshifted $\approx 10^3 \text{ km s}^{-1}$ we find that FWHM of BLR $H\beta$ remains almost constant and in the range $4300-4800 \text{ km s}^{-1}$. Unlike Pop. A sources, Pop. B objects show CIV profiles that closely match those of $H\beta$. A VBLR component is very prominent in $B1^+$ objects and necessary to obtain a reasonable fit of the whole CIV profile.

If we are correct in assuming that this is the classical reverberating accretion disk component then we can again compute BH masses for Pop. B sources. The values do not come down as much as might be expected because the sources with the largest VBLR correction are also the most luminous. However this tells us that the Pop. A-B difference is not driven so much by FWHM $H\beta$ but rather by the presence of the VBLR component that is very weak or absent in Pop. A quasars. Figure 4 represents the strongest evidence to date for the BLR+VBLR interpretation of the Pop. B $H\beta$ line profile. There is a widespread idea that a double peaked accretion disk component is hidden in the profile and indeed NGC5548 the most reverberated source shows it. If present in all or most sources this disk component does not show up in our high S/N median composite. It is apparently hidden

by an unshifted (or slightly blueshifted) BLR component and the redshifted VBLR. We consider it virtually impossible that an anomaly in the FeII emission (or error in the FeII modeling) could produce this feature. It represents a major challenge to our ideas about structure and kinematics of the central region in quasars.

Paralleling our discussion of Pop. A sources we note that Pop. B quasars show no soft X-ray excess or CIV blueshift (Figure 2). If their presence is a signature of a stable BLR under high accretion in Pop. A sources then the BLR is much less prominent in Pop. B sources that host an additional VBLR emitting component. Isolating the BLR component of $H\beta$ as a virial estimator in Pop. B suggests that BH masses are on average larger ($\log(M_{BH}[M_{\odot}]) \approx 7-10$) and, especially, that Eddington ratio is lower ($\log(L_{BOL}/L_{EDD}) \approx -0.7$ to -1.4) than in Pop. A.

6. Meaning of a Pop. A-B Dichotomy and VBLR?

These questions are asked together because we think they are related. After all the appearance of the VBLR component near $\text{FWHM } H\beta = 4000 \text{ km s}^{-1}$ is one of the strongest arguments for a Pop. A-B dichotomy (Sulentic et al. 2000b, 2007). We therefore conclude that the dichotomy is real and likely related to a critical Eddington ratio below which BLR structure undergoes a significant change in geometry and kinematics (see also Collin et al. 2006; Bonning et al. 2007; Kelly et al. 2008; Hu et al. 2008). If a critical L_{BOL}/L_{EDD} is the driver then how does the VBLR relate to this change? So far we can infer four VBLR characteristics: 1) it is very broad, 2) it is highly redshifted, 3) it is reasonably well fit by a symmetric Gaussian, and 4) it becomes more prominent at higher luminosity (due to a weakening of the central BLR component). The equivalent width of the VBLR component is roughly constant over six decades of luminosity, which implies production in optically-thick, photoionized gas. We can identify three classes of models that might explain the VBLR: a) gravitation (clues 1 and 2), b) infall (clue 2), c) photon downshifting through scattering processes (clues 1, 2 and 4). Inferred BH mass values are not large enough to make it likely that the VBLR arises close enough to the BH and clue 3 argues against this interpretation as well. We think that b) or c) likely provides the solution and we encourage to pursue them just as we are doing.

References

- Bachev, R., Marziani, P., Sulentic, J. W., Zamanov, R., Calvani, M., Dultzin-Hacyan, D. 2004 *ApJ*, 617, 171
- Bonning, E. W., Cheng, L., Shields, G. A., Salviander, S., Gebhardt, K. 2007, *ApJ*, 659, 211
- Boroson, T. A. & Green, R. F. 1992, *ApJS*, 80, 109
- Collin, S., Kawaguchi, T., Peterson, B. M., Vestergaard, M. 2006, *A&A*, 456, 75
- Hu, C., Wang, J.-M., Ho, L. C., Chen, Y.-M., Zhang, H.-T., Bian, W.-H., Xue, S.-J. 2008, *ApJ*, 687, 78
- Kelly, B. C., Bechtold, J., Trump, J. R., Vestergaard, M., Siemiginowska, A. 2008, *ApJS*, 176, 355
- Marziani, P., Sulentic, J. W., Zwitter, T., Dultzin-Hacyan, D., Calvani, M. 2001, *ApJ*, 558, 553
- Marziani, P., Zamanov, R. K., Sulentic, J. W., Calvani, M. 2003a, *MNRAS*, 345, 1133
- Marziani, P., Sulentic, J. W., Zamanov, R., Calvani, M., Dultzin-Hacyan, D., Bachev, R., Zwitter, T. 2003b, *ApJS*, 145, 199
- Marziani, P., Sulentic, J. W., Stirpe, G. M., Zamfir, S., Calvani, M. 2009, *A&A*, 495, 83
- Sulentic, J. W., Zwitter, T., Marziani, P., Dultzin-Hacyan, D. 2000a, *ApJ*, 536, L5
- Sulentic, J. W., Marziani, P., Dultzin-Hacyan, D. 2000b, *ARA&A*, 38, 521
- Sulentic, J. W., Marziani, P., Zamanov, R., Bachev, R., Calvani, M., Dultzin-Hacyan, D. 2002, *ApJ*, 566, L71
- Sulentic, J. W., Bachev, R., Marziani, P., Negrete, C. A., Dultzin, D. 2007, *ApJ*, 666, 757
- Wang, T., Brinkmann, W., Bergeron, J. 1996, *A&A*, 309, 81
- Zamanov, R., Marziani, P., Sulentic, J. W., Calvani, M., Dultzin-Hacyan, D., Bachev, R. 2002, *ApJ*, 576, L9
- Zamfir, S., Sulentic, J. W., Marziani, P. 2008, *MNRAS*, 387, 856
- Zamfir, S., Sulentic, J. W., Marziani, P. 2009, submitted to *MNRAS*
- Zhou, H., Wang, T., Yuan, W., Lu, H., Dong, X., Wang, J., Lu, Y. 2006, *ApJS*, 166, 128